Materials Science in Semiconductor Processing 169 (2024) 107934

Contents lists available at ScienceDirect

Materials Science in Semiconductor Processing

journal homepage: www.elsevier.com/locate/mssp

Employment of dopant-free fluorene-based enamines as innovative hole transport materials to boost the transparency and performance of Sb_2S_3 based solar cells

Nimish Juneja [a], Sarune Daskeviciute-Geguziene [b], Nicolae Spalatu [a], Sreekanth Mandati [a], Atanas Katerski [a], Raitis Grzibovskis [c], Aivars Vembris [c], Smagul Karazhanov [d], Vytautas Getautis [b], Malle Krunks [a,*], Ilona Oja Acik [a]

[a] Department of Materials and Environmental Technology, Tallinn University of Technology, Ehitajate tee 5, Tallinn, 19086, Estonia
[b] Department of Organic Chemistry, Kaunas University of Technology, Kaunas, LT-50254, Lithuania
[c] Institute of Solid State Physics, University of Latvia, Kengaraga Str. 8, Riga, LV-1063, Latvia
[d] Institute for Energy Technology (IFE), P.O Box 40, Kjeller, NO 2027, Norway

ARTICLE INFO

Keywords:
Antimony sulfide
Hole transport material
Semitransparent solar cells
Photovoltaics

ABSTRACT

Antimony sulfide (Sb_2S_3) with bandgap of ca. 1.7 eV is a promising absorber material for indoor and semi-transparent photovoltaic devices. However, the high cost of commonly used hole transport materials (HTMs) may impede the advancement of this technology. In this study, dopant-free fluorene-based enamines with different aliphatic chain length synthesized by a simple chemical method are used for the first time as HTMs in Sb_2S_3 solar cell. The study investigates impact of HTM type and layer thickness on the performance of Sb_2S_3 solar cells. The solar cells are fabricated in superstrate configuration with Sb_2S_3 absorber layer deposited through ultrasonic spray pyrolysis and HTM layer applied via spin-coating. Energy level diagrams, constructed using ionization potential values of cell component layers, indicate agreeable band offsets validating the suitability of new HTMs for Sb_2S_3 solar cells. Both the aliphatic chain length in HTM and layer thickness influence the power conversion efficiency (PCE) of the device, layer thickness of 20–25 nm is identified as optimal. Solar cells with new HTMs demonstrate higher PCEs (3.9–4.3%) compared to the reference device employing P3HT (3.8%). Moreover, Sb_2S_3 cells with new HTMs without metal contact exhibit 20% increase in average visible transmittance, underscoring their potential in semi-transparent applications.

1. Introduction

Metal chalcogenides like Cadmium Telluride (CdTe), [1,2] Cu(In,Ga)Se_2 (CIGS), [3,4] have been successful as light harvesting materials due their high absorption coefficients and excellent optoelectronic properties. Thin-film solar cells based on CdTe and CIGSSe, have reached power conversion efficiencies (PCE) of 22.1% and 23.4%, respectively [5,6]. However, in a long term, the large-scale implementation of some of these established PV technologies might face some barriers related to the availability of expensive In and Ga elements. In addition to traditional inorganic thin film technologies, antimony chalcogenides, such as Sb_2S_3, Sb_2Se_3 and $Sb_2(S_{1-x}Se_x)_3$ have demonstrated strong photon harvesting ability, high chemical stability, nontoxicity and benign synthesis and have recently emerged as viable photovoltaic absorbers [7–11]. In a short period of time the PCEs of Sb_2S_3, Sb_2Se_3 and $Sb_2(S,Se)_3$ based solar cells have reached 8.0%, 10.57%, 10.75%, respectively, [12–14] making them promising candidates for next-generation PV in the family of antimony chalcogenides. Sb_2S_3 possesses a high absorption coefficient of approximately 10^5 cm^{-1} at 450 nm and a relatively wide bandgap of 1.7–1.8 eV [11,15–17]. Consequently, it is a suitable absorber material for both single junction solar cells as well as for advanced device concepts, such as tandem devices. Sb_2S_3 based PV devices could be principally used in wide range of applications such as solar windows in building-integrated photovoltaics (BIPV), [11,17] semitransparent electronics and due to excellent low-light harvesting ability also in standalone indoor PV [10].

Sb_2S_3 thin films can be deposited using a range of physical and chemical methods, avoiding the formation of secondary phases. The

* Corresponding author.
E-mail address: malle.krunks@taltech.ee (M. Krunks).

https://doi.org/10.1016/j.mssp.2023.107934
Received 29 June 2023; Received in revised form 27 September 2023; Accepted 23 October 2023
Available online 31 October 2023

chemical deposition techniques include mainly chemical bath deposition (CBD), [18,19] ultrasonic-spray pyrolysis (USP), [11,20,21] spin coating, [22,23] and atomic layer deposition (ALD) [16,24]. Different physical deposition techniques are being employed for the preparation of Sb_2S_3 absorbers, including sputtering, [25,26] thermal evaporation, [27,28] and closed space sublimation [29,30]. The composition of the Sb_2S_3 solar cell stack is similar to perovskite solar cells, encompassing an electron transport layer (ETL), an absorber layer, a hole transport material (HTM), and metal front and back contacts. In a recent study by Wang et al., the utilization of CBD for the deposition of Sb_2S_3 has led to fabrication of solar cells yielding a PCE of 8.0% [12]. Eensalu et al., fabricated solar cells using USP for the preparation of Sb_2S_3 and obtained the PCE of 5.5% [17]. Han et al., fabricated solar cell devices with spin coating for the deposition of Sb_2S_3 and has obtained PCE of 7.1% [31]. Büttner et al., fabricated solar cells with PCE of 5.1% while using ALD for preparation of the absorber Sb_2S_3 [32].

To fabricate semi-transparent solar cells based on Sb_2S_3, it is crucial to ensure an absorber thickness of less than 100 nm, and in this perspective, USP and ALD can be employed to deposit semitransparent absorber layer [11,17,33]. USP is a low-cost, area-scalable and a high throughput solution-based technique [11,17]. In previous studies, we have demonstrated that compact Sb_2S_3 films can be deposited using a two-step process [11,17,20]. Firstly, amorphous Sb_2S_3 films are deposited at relatively low temperature of around 200 °C. This is followed by crystallization of the absorber layer by thermal annealing in vacuum [11,17,20] or in N_2 at temperature up to 250 °C [20,21] resulting in PCE of 4–6%. Apart from the quality of the absorber in the solar cells, another key component in the solar cell device is the HTM. The presence of HTM aids in effective extraction and the transport of photogenerated holes to the metal back contact. It prevents the diffusion of metal into the absorber, reduces charge recombination losses at the interface between the absorber and HTM, and provides encapsulation for the absorber. The most popular conjugated polymers as HTMs in Sb_2S_3 based solar cells are *poly(3-hexylthiophene)* (P3HT), [11,16,17,34] *2,2′,7,7′-tetrakis[N,N-di(4-methoxyphenyl)amino]-9,9′-spirobifluorene* (Spiro-OMeTAD), [12,32,35] *poly(3,4-ethylenedioxythiophene)poly(styrenesulfonate)* [36,37] (PEDOT:PSS) and *poly[2,6-(4,4-bis(2-ethylhexyl)-4H-cyclo-penta[2,1-b;3,4-b′]dithiophene)-alt-4,7-(2,1,3 benzothiadiazole)]* (PCPDTBT) [38,39].

Wang et al., prepared solar cells (FTO/CdS/Sb_2S_3/Spiro-OMeTAD/Au) yielding a PCE of 8.0% using Spiro-OMeTAD as HTM [12]. Eensalu et al., fabricated solar cells using USP for the preparation of Sb_2S_3 with P3HT as HTM (ITO/TiO_2/Sb_2S_3/P3HT/Au) and obtained the PCE of 5.5% [17]. On a similar note, Choi et al. achieved a PCE of 7.5% by using CBD for Sb_2S_3 deposition and utilized HTMs - PCPDTBT and PEDOT:PSS in the solar cell configuration of FTO/mp-TiO_2/Sb_2S_3/PCPDTBT/PEDOT:PSS/Au [19]. Furthermore, alternative inorganic materials such as NiO_x, [40] CuSCN, [41,42] and V_2O_5 [43] have also been employed as HTMs in Sb_2S_3 based solar cells. Despite the fact that conventionally employed HTMs such P3HT, Spiro-OMeTAD, PCPDTBT, etc. have been successfully used, their low synthesis yield and high manufacturing cost may limit the viability of Sb_2S_3 solar cells. Spiro-OMeTAD is synthesized in a multi-step reaction scheme that requires a low temperature (−78 °C) and sensitive (*n*-butyllithium or Grignard reagents) reagents [44,45]. Additionally, the use of Spiro-OMeTAD in the solar cell requires its doping with Li-based salt to improve its hole transporting capability. This adds to the cost and reduces the stability of the devices as the dopant Lithium bis(trifluoromethylsulphonyl)imide (LiTFSI) is hygroscopic [46]. The band gap of 1.8 eV in P3HT introduces parasitic absorption losses in the device, consequently reducing the transparency of the solar cells [11,17,34]. Moreover, the processing of P3HT necessitates an additional activation step at around 170 °C [11,17]. Considering the limitations listed above, there is an obvious need to search alternative HTMs combining properties such as optical transparency, efficient charge extraction and low cost.

Thus, the objective of this study is to propose new HTMs as alternative options to conventional HTMs like Spiro-OMeTAD and P3HT for Sb_2S_3 solar cells, targeting semi-transparency, appropriate band alignment and enhanced solar cell performance. In the present study, fluorene-based enamines are synthesized, characterized, and their potential as an HTM in Sb_2S_3 based solar cells is explored. V1275 (*N^2,N^2,N^7,N^7-tetrakis[2,2-bis(4-methoxyphenyl)vinyl]-9H-fluorene-2,7-diamine), V1235 (N^2,N^2,N^7,N^7-tetrakis[2,2-bis(4-methoxyphenyl)vinyl]-9,9-dipropyl-9H-fluorene-2,7-diamine), and V1461 (N^2,N^2,N^7,N^7-tetrakis[2,2-bis(4-methoxyphenyl)vinyl]-9,9-dinonyl-9H-fluorene-2,7-diamine)* that are belonging to the enamine family with a central fluorene scaffold, differ from each other by the length of aliphatic chain. These compounds can be produced in a straightforward condensation reaction from commercially available and cheap materials. The synthesis cost of V-series HTMs are considerably lower, estimated to be around 10–20 €/g, in contrast to conventional HTMs like Spiro-OMeTAD (approximately 90 €/g) [47] and P3HT (approximately 45 €/g) [48]. The two out of the three proposed HTMs – namely V1275 and V1235 have previously been utilized as dopant-free HTMs in perovskite solar cells, resulting in PCE of 17.1% and 16.6%, respectively [49]. V1461 with its -nonyl chain is a newly synthesized material. In summary, the three materials - V1275, V1235 and V1461 are tested as HTMs for the first time in Sb_2S_3 based solar cells.

The solar cell stacks are fabricated in superstrate configuration glass/FTO/TiO_2/Sb_2S_3/HTM/Au. USP is used for the deposition of TiO_2 and Sb_2S_3 layers, while the HTMs are applied using the spin-coating technique. In order to investigate the influence of HTM layer thickness on the performance of solar cells, a systematic approach is employed, wherein the thickness of the layer is optimized by changing the concentration of the HTM precursor solution. The solar cell performance with V-series HTMs is compared to that of solar cells with reference HTM - P3HT. Combining the different characterization techniques for material and device, new insights are provided on the functionality of the V - series HTMs in correlation with the performance of Sb_2S_3 based semi-transparent device.

2. Experimental

2.1. Materials

The chemicals used for the synthesis of the HTMs - *N^2,N^2,N^7,N^7-tetrakis[2,2-bis(4-methoxyphenyl)vinyl]-9H-fluorene-2,7-diamine (V1275), N^2,N^2,N^7,N^7-tetrakis[2,2-bis(4-methoxyphenyl)vinyl]-9,9-dipropyl-9H-fluorene-2,7-diamine (V1235), and N^2,N^2,N^7,N^7-tetrakis[2,2-bis(4-methoxyphenyl)vinyl]-9,9-dinonyl-9H-fluorene-2,7-diamine (V1461)* are purcha sed from Sigma-Aldrich and used as received without further purification. A detailed description of the materials related to HTM synthesis are presented in Supporting Information (SI) file, in Table S1. FTO substrate (7 Ω/sq.), Titanium(IV) tetraisopropoxide (TTIP) – Acros Organics (99 wt%), Acetylacetone - Acros Organics (99 wt%), Ethanol - Estonian Spirit (96.6 vol%), Methanol - Sigma-Aldrich (99.9 vol%), Antimony trichloride - Sigma-Aldrich (99.99 wt%), Thiourea - Sigma-Aldrich (99 wt%), Chlorobenzene - Sigma-Aldrich (99.5 vol%), and Poly(3-hexylthiophene-2,5-diyl) (P3HT) Sigma-Aldrich (Regio regular, >90%) are used as received.

2.2. Methods

2.2.1. Fabrication of solar cell

Solar cell devices are fabricated using the same experimental procedure as described elsewhere [20,21]. In brief, Fluorinated tin oxide (FTO) coated glass with a sheet resistivity of 7 Ω sq^{-1} is used as a substrate. The device configuration and schematic representation of the standard process used to fabricate Sb_2S_3 solar cells is presented in SI, in Fig. S1. The glass/FTO substrates (20 mm × 20 mm) were meticulous cleaned with a procedure, which includes extensive rinsing with deionized water, ethanol, and methanol. This is followed by immersion in boiling deionized water for a duration of 15 min. Finally, the substrates are dried by N_2 gas. The TiO_2 precursor solution is prepared by

combining 0.2 M TTIP and 0.2 M acetylacetone in solvent ethanol. The ETL - TiO_2, and the absorber - Sb_2S_3 are deposited onto the cleaned glass/FTO substrates using a USP setup. Deposition of films by USP involves spraying the aerosol onto the substrate using compressed air as the carrier gas. During the deposition, the substrates are maintained at a temperature of 340 °C using a hot plate. The as-deposited TiO_2 samples are then subjected to annealing on a hot plate in air at a temperature of 450 °C for a duration of 30 min. For the preparation of the Sb_2S_3 precursor solution, 180 mM of thiourea is dissolved in 60 mM of antimony chloride ($SbCl_3$) within 120 mL of methanol. Similar to TiO_2, the absorber is deposited using USP method, with the substrate maintained at a temperature of 198 °C. After deposition, the amorphous Sb_2S_3 thin films underwent annealing at 250 °C for 5 min within a N_2 atmosphere. Subsequently, the HTMs are applied onto the Sb_2S_3 films through spin coating (3000 rpm at 30s), utilizing the respective precursors dissolved in chlorobenzene. The concentrations of the three HTMs - V1275, V1235, and V1461 - are systematically altered. For P3HT, the standard concentration of 1% wt. is used [20,21]. Samples with P3HT need an additional activation step in vacuum at 170 °C for 5 min, whereas no such step is needed for the new HTMs. Sequentially, 80–100 nm of Au back contact is thermally evaporated through a shadow mask under a pressure of about 10^{-4} Pa. The active contact area of the fabricated device is 7.06 mm^2.

2.2.2. Characterization of synthesized HTMs and fabricated solar cells

The structure of the HTMs was confirmed using the H NMR measurements. Details are introduced in SI, section S2, and the NMR and mass spectroscopy (MS) spectra are presented in Figs. S2–S4. The HTMs were characterized comprehensively using TGA, DSC, and absorption spectroscopy. DSC data is presented in SI, in Fig. S4. Optical absorption and Photoluminescence spectra of the HTMs were measured in THF solution (10^{-4} M). Details are given in SI, section S1. The hole drift mobility of the novel HTMs was determined using the time of flight (ToF) method on "sandwich" type samples (ITO/HTM/Al) as described in detail in SI, in section S3. Ionization potential of the constituent layers was measured using the photoelectron yield spectroscopy (PYS) method described in detail in SI, in section S4. The total transmittance and total reflectance spectra of the stacks - glass/FTO/HTM and glass/FTO/TiO_2/Sb_2S_3/HTM, were measured using an ultraviolet–visible (UV-VIS) spectrophotometer within the 250–1100 nm range. In order to determine the optical bandgap values of the HTMs, the total transmittance spectra of HTM films was utilized to calculate the absorption coefficient (α) and derive the corresponding bandgap values (E_g) through Tauc plots. Additionally, the work function of the Au metal contacts was measured employing a Kelvin probe.

The electrical characterization of the solar cells was performed by measuring their current-voltage (I–V) characteristics using a Wavelabs LS-2 LED solar simulator (AM1.5G, 100 mW cm^{-2}). To measure the external quantum efficiency (EQE) spectra of the fabricated solar cells, a Newport 69911 system was employed. Furthermore, the surface and cross-sectional morphologies of the fabricated devices were examined using a Zeiss HR FESEM Ultra 55.

3. Results and discussion

3.1. Synthesis and properties of HTMs

The HTM compounds – V1275, V1235 and V1461 were synthesized using one-pot or two-step reactions performed under ambient conditions. Synthesis route is presented in Fig. 1a. Materials with high yields and purity could be synthesized. Commercially available reagents 2,7-diamino fluorene and 2,2-bis(4-methoxyphenyl) acetaldehyde were used in the presence of camphor sulfonic acid to yield V1275 [49] V1275 on further reaction with alkylating agents bromopropane and bromononane yielded propyl- and nonyl-substituted fluorene enamines V1235 and V1461. The chemical composition of the produced compounds is confirmed by NMR and MS spectroscopy (see details in SI, Figs. S2–S4). The chemical structures of V1275, V1235 and, V1461 is presented in Fig. 1b, c and d, respectively.

To study the thermal stability of the synthesized HTMs, thermogravimetric analysis (TGA) was performed and is presented in Fig. 2a. Thermal and optoelectronic properties V1275 and V1235 have been published in a previous study [49]. Since V1461 is a newly synthesized material with a longer aliphatic chain (nonyl substituted), its properties are compared to V1275 (with no aliphatic chain) and V1235 (propyl substituted). All the three HTM compounds – V1275, V1235 and V1461, decompose at temperatures of around 400 °C. V1275 has the highest thermal stability with a decomposition temperature (T_{dec}) of 403 °C. It should be noted that V1275 and V1235 exist in both the crystalline and amorphous states, in contrast to V1461, which is amorphous. The glass

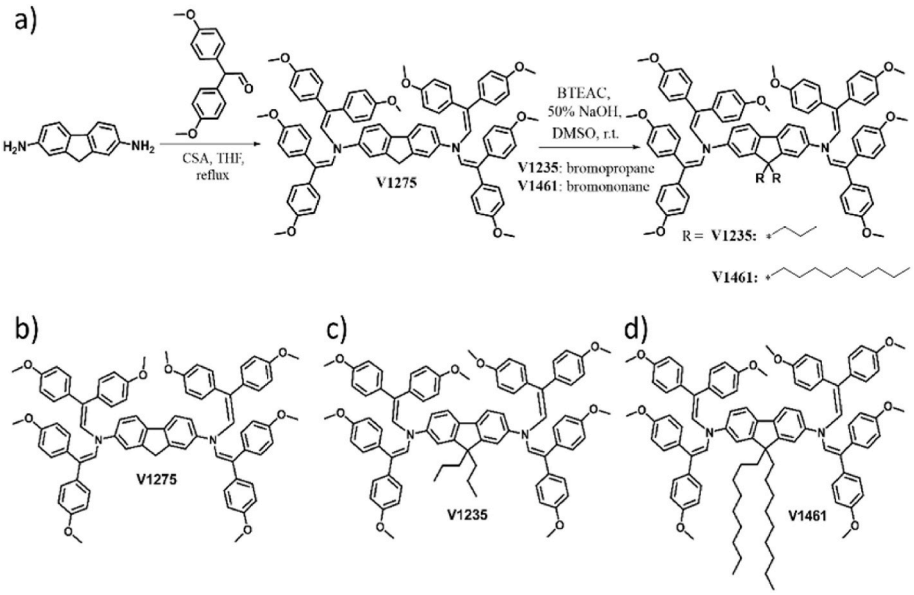

Fig. 1. a) Synthetic route to V1275, V1235 and V1461. b) N2,N2,N7,N7-tetrakis[2,2-bis(4-methoxyphenyl)vinyl]-9H-fluorene-2,7-diamine (V1275). c) N2,N2,N7,N7-tetrakis[2,2-bis(4-methoxyphenyl)vinyl]-9,9-dipropyl-9H-fluorene-2,7-diamine (V1235), d) N2,N2,N7,N7-tetrakis[2,2-bis(4-methoxyphenyl)vinyl]-9,9-dinonyl-9H-fluorene-2,7-diamine (V1461).

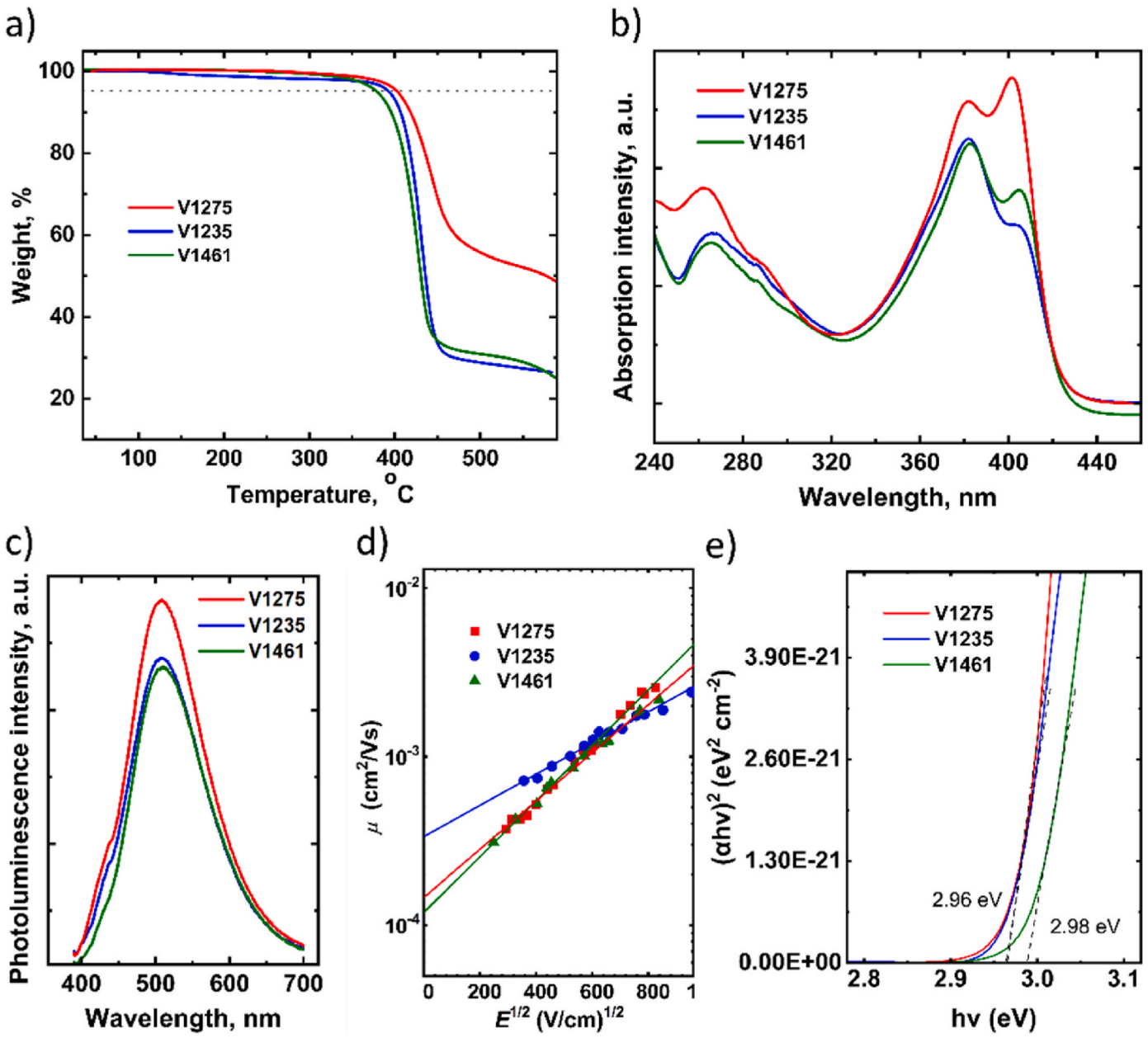

Fig. 2. a) Thermogravimetric analysis (TGA) data (heating rate of 10 °C/min, N_2 atmosphere). b) UV–Vis absorption spectra of V-series HTMs in THF solutions (10^{-4} M). c) Photoluminescence spectra of the HTMs in THF solution (10^{-4} M). d) Electric field dependencies of the hole-drift mobility in the studied HTMs. e) Tauc's plots of V1275, V1235 and V1461 thin films.

transition temperatures (T_g) for V1275 and V1235 are 150 and 120 °C, respectively, indicating stability of the amorphous state of these molecules. The differential scanning calorimetric (DSC) curves of new HTMs is presented in SI, in Fig. S5. The melting (T_m), crystallization (T_c) and glass transition (T_g) temperatures, together with the decomposition temperatures (T_{dec}) of HTMs are summarized in Table 1. Next, to characterize the optoelectronic properties of the HTMs, optical absorption and photoluminescence (PL) spectra were recorded for HTMs in THF solution, and are presented in Fig. 2b and c, respectively. All the three HTMs exhibit two main absorption peaks at about 260 nm and 400 nm. The absorption peak at shorter wavelength of 260 nm corresponds to the localized π-π* transitions. The less intense absorption peak at the shorter wave-length corresponds to localized π–π* transitions while the longer wavelength absorption arises from more intensive delocalisation from the conjugated scaffold and is assigned to n–p* transitions [49]. The conjugation has not been affected by modifications to the different

Table 1
Thermal, optical and electrical properties of HTMs - V1275, V1235 and V1461.

HTM	T_m [°C]	T_c [°C]	T_g [°C]	T_{dec} [°C]	λ_{abs} [nm]	λ_{em} [nm]	μ_0 [$cm^2 V^{-1} s^{-1}$]	E_g [eV]
V1275	255	–	150	403	262, 381, 401	508	1.2×10^{-4}	2.96
V1235	273	159	120	399	266, 382, 404	509	3.3×10^{-4}	2.96
V1461	–	–	99	370	265, 382, 405	511	1.5×10^{-4}	2.98

aliphatic chain length, and thus the spectra of all molecules are nearly the same. As seen in Fig. 2c, the PL spectra of all the three synthesized HTM molecules have a peak at 510 nm. The compounds have absorption peaks at 400 nm and emission peak at 510 nm, which depicts large Stokes shifts of approximately 100 nm for all the molecules [49].

Melting (T_m), crystallization (T_c), glass transition (T_g) and decomposition (T_{dec}) temperatures observed from DSC and TGA, respectively (10 °C/min, N_2 atmosphere). Optical absorption (λ_{abs}) and optical emission (λ_{em}) peak positions in spectra as measured in THF solution (10^{-4} M). Hole drift mobility (μ_0) value at zero field strength and the bandgap (E_g) estimated using the Tauc plot.

Additionally, to study the hole-mobility of the HTMs, time of flight (TOF) technique is used. High hole mobility is required in HTM for the efficient transport of the holes to the back contact [49]. Fig. 2d shows how the mobility of a hole is dependent on the strength of the electric field. When compared to the other members of the fluorene series, the propyl substituted V1235 has the highest zero-field hole mobility (μ_0) of 3.3×10^{-4} cm^2 V^{-1} s^{-1}. The zero-field hole drift mobility for V1275 and V1461 was found to be at 1.2×10^{-4} cm^2 V^{-1} s^{-1} and 1.5×10^{-4} cm^2 V^{-1} s^{-1}. The V- series HTMs have hole mobility values comparable to those of P3HT ($\mu_0 = 2 \times 10^{-4}$ cm^2 V^{-1} s^{-1}) [50] and Spiro-OMeTAD ($\mu_0 = 1.3 \times 10^{-4}$ cm^2 V^{-1} s^{-1}) [49]. The incorporation of longer chains into the molecular structure is risky as the mobility of charge carriers can decrease due to the decreasing concentration of photoconductive chromophores [49]. However, the opposite situation is possible when molecules are ordered more due to the presence of the chains and in this case the mobility of charge carriers increases. For example, hole mobility in V1235 at weak field is better than that in V1275, though the concentration of chromophores is the highest in the latter HTM. It can be assumed, that the chains make steric orientation of the molecules more ordered and the obtained layers are of better quality (without pin-holes) [49]. Also, the drift mobility in V1461 is lower due to the presence of long chains, which significantly decrease concentration of chromophores. Thus, there is a correlation between the chain length and HTM performance. The E_g values were determined from the Tauc plots as presented in Fig. 2e for V1275 and V1235 were similar, 2.96 eV, and for nonyl substituted V1461, E_g was 2.98 eV.

3.2. Application of HTMs in solar cells

Thin film Sb_2S_3 based solar cells were fabricated in the superstrate configuration (glass/FTO/TiO_2/Sb_2S_3/HTM/Au) as presented in Fig. 3a. The HTMs – V1275, V1235, V1461, and P3HT are spin coated. From our previous study, we observed that P3HT – 1% wt. gives the thickness of 80 nm, which is an optimal value for the most efficient solar cell stack [11,17]. As the V-series HTMs are being used in Sb_2S_3 based solar cells for the first time, therefore the conditions for obtaining a layer of suitable thickness for efficient solar cell must be determined. The layer thickness was changed by varying the HTM concentration in the solution.

Fig. 3b, c and d show the current density-voltage (J-V) characteristics of solar cells with concentration variation for the HTMs - V1275, V1235 and V1461. Initially, a concentration of 15 mM of HTM precursor solution was used to fabricate solar cells as this concentration has been previously employed for the successful production of efficient perovskite solar cells [49]. As seen from J-V characteristics, the cell performances are low using 15 mM HTM solutions, yet the dilution of solutions allows to obtain higher J_{SC} and V_{OC} for all the devices. For example, V_{OC} increased from 490 mV to 570 mV, J_{SC} increased from 0.8 to 12.5 mA/cm^2 and PCE from 0.8 to 3.0% when reducing V1235 concentration

Table 2
Effect of HTM V1235 solution concentration on solar cell output characteristics.

V1235 conc. [mM]	V_{OC} [mV]	J_{SC} [mA/cm^2]	FF [%]	PCE [%]	R_S [Ω. cm^2]
15	490	0.8	21	0.8	23
4	570	12.5	42	3.0	2.1
2	587	15.5	47	4.3	1.3
1	582	14.1	45	3.7	1.0

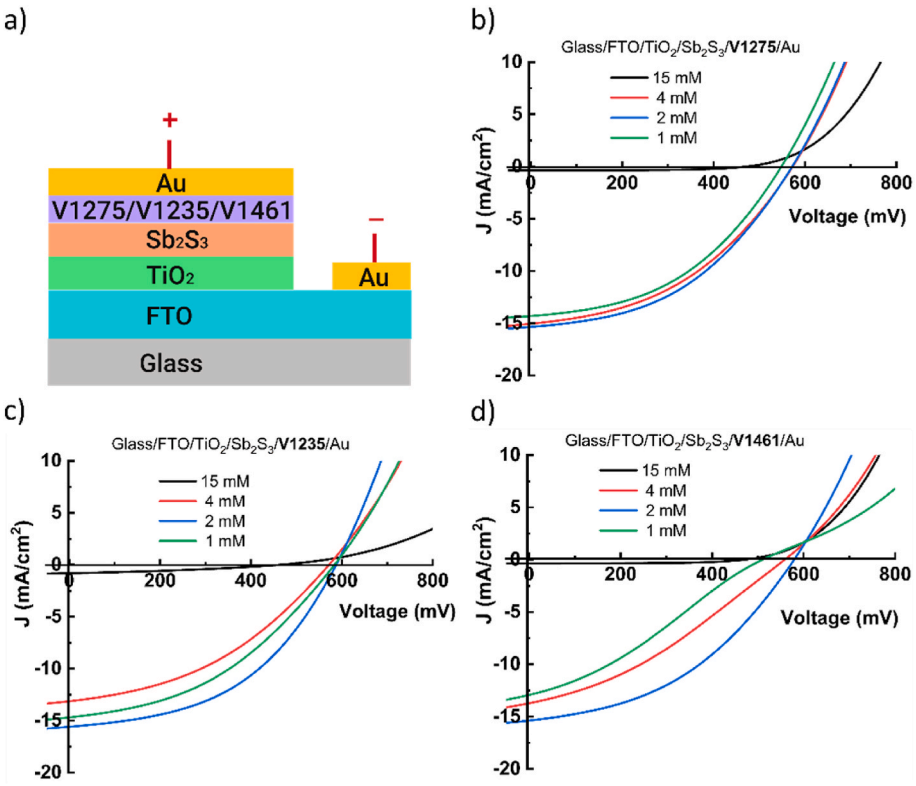

Fig. 3. a) Sb_2S_3 solar cell configuration and J-V curves of Sb_2S_3 solar cells with HTMs, b) V1275, c) V1235, and d) V1461.

from 15 to 4 mM (Fig. 3c, Table 2). Further dilution to 2 mM results in a solar cell demonstrating V_{OC} of 587 mV, J_{SC} of 15.5 mA/cm^2 and PCE of 4.3%. Following dilution to 1 mM resulted in a drop in J_{SC} to 14.1 mA/cm^2 accompanied by a slight drop in V_{OC} to 582 mV, and a decrease in PCE to 3.7%. Very similar trend of the solution concentration on solar cell output characteristics was recorded using V1461 as HTM (Fig. 3d). In case of V1275, the effect HTM solution concentration on cell output characteristics was less pronounced although some drop in V_{OC} and J_{SC} were also recorded when using 1 mM solution (Fig. 3b). The highest PCE values were recorded for the cells with hole transport layers obtained from 2 mM solution of all V-series HTMs (Fig. 3b, c, d).

SEM cross-sectional images of solar cells incorporating HTM layers derived from V1235 at different precursor concentrations are shown in SI, in Fig. 4. As expected, the HTM layer thicknesses decrease when the solution concentration is reduced, for example, V1235 – 15 mM gave a thickness of ca. 120 nm, 2 mM of ca. 25 nm and 1 mM of ca. 15 nm. Thus, a drop in R_S from 23 to 1.0 Ω cm^2 correlates with a decrease in HTM layer thickness from 120 nm to 15 nm while reducing solution concentration from 15 to 1 mM (Table 2). According to J-V curves (Fig. 3b–d), the V_{OC}, J_{SC} and FF are lowered when HTM layer from heavily diluted 1 mM solutions is applied, resulting in a decrease of solar cells performances as also observed in a previous study using N^2,N^2,N^7,N^7-tetrakis[2,2-bis(4-methoxyphenyl)vinyl]-9,9- dihexyl-9*H*-fluorene-2,7-diamine (V1236) as HTM on Sb_2S_3 absorber [20]. It is likely that HTM layers with thickness of around 15–20 nm do not cover the absorber layer uniformly and may contain pinholes allowing direct contact of the gold electrode to the active layer. It has been also reported that poor layer formation could be controlled by the HTM molecular structure [51]. In our study, the cell with V1275 that has no aliphatic chain in its structure showed the smallest decline of output parameters at HTM layer low thicknesses (Fig. 3).

In order to understand the energy levels alignment of the studied HTMs (V1275, V1235 and V1461) with that of the absorber material Sb_2S_3 and metal back contact Au, photoemission spectroscopy was used to measure the ionization potential (I_p) of the constituent layers within the solar cell stack, namely FTO, TiO_2, Sb_2S_3 and the HTMs. Experimental data for I_p determination for HTMs - V1275, V1235, V1461 are presented in Fig. 5a, b, and c, respectively. The I_p values (HOMO levels) for V1275, V1235 and V1461, were found to be at −4.92, −4.80, and −4.94 eV, respectively, that are close to the HOMO levels reported for HTMs such as Spiro-OMeTAD (−5.2 eV) and PCPDTBT (−5.2 eV) [10]. I_p values for P3HT, TiO_2 and Sb_2S_3 were measured in our previous study [20] and were −4.60 eV, −7.40 eV and – 5.10 eV, respectively. Taking into account the band gap energies measured for V1275, V1235, V1461 (Table 1), the LUMO levels of V-series HTMs are at −2.8 eV, −2.1 eV, −2.0 eV, and −2.1 eV, respectively. The band energy diagram is presented in Fig. 5d.

In order to ensure a comprehensive evaluation, solar cells utilizing V1275 – 2 mM, V1235 – 2 mM, V1461 – 2 mM, and the commonly used HTM - P3HT were fabricated within the same experimental batch. Additionally, to comprehend the influence of HTMs, control solar cell devices were fabricated devoid of any HTM, following the stack configuration of glass/FTO/TiO_2/Sb_2S_3/Au. The J-V characteristics of champion cells with no HTM and HTMs - P3HT – 1% wt., V1275 – 2 mM, V1235 – 2 mM and V1461 – 2 mM are presented in Fig. 6a. The solar cell results are shown in Table 3. The reference device fabricated without an HTM exhibited a V_{OC} of 450 mV, J_{SC} of 12.8 mA/cm^2, FF of 0.4 and a PCE of 2.1%. Application of HTMs significantly increases the V_{OC} value compared to the reference device. For example, V_{OC} of 650 mV was recorded for a solar cell with P3HT as HTM, and V_{OC} at around 580 mV was recorded for solar cells with V-series HTMs being in correlation with enhanced shunt resistance (R_{SH}) of the devices (Table 3). As Sb_2S_3 absorber exhibits the valence band edge (VBE) at −5.1 eV and the conduction band edge (CBE) at −3.4 eV, then in a device without HTM (TiO_2/Sb_2S_3/Au), there is no barrier for electrons to flow from the conduction band of Sb_2S_3 to the Au back contact (Work function of Au −5.1 eV). This enables the recombination resulting in lower V_{OC} and FF.

Applying an HTM reduces the recombination losses as electron affinity values of the HTM molecules (−2.0 or −2.1 eV, Fig. 5d) are smaller than the CBE of Sb_2S_3 at −3.4 eV. Therefore, the electron transfer from the absorber to the HTMs is effectively blocked. According to the VBE of Sb_2S_3 at −5.1 eV and that of V-series HTMs at −4.9 eV, the transfer of photogenerated holes from the absorber - Sb_2S_3 to HTM is feasible, although HTMs with higher HOMO levels are expected to perform better. The PCE obtained for the optimized concentrations of V1275 and V1461 were 3.9% and 3.7%, respectively, comparable to the cell with P3HT (3.8%), however, the highest PCE of 4.3% was recorded for solar cell device with HTM -V1235. Next, the external quantum efficiency (EQE) response of the devices were performed and the plot is presented in Fig. 6b. Solar cells incorporating the V-series HTMs demonstrated a higher EQE spectral response than cells with P3HT across the entire wavelength range. The EQE response of the solar cell with P3HT exhibits a concavity within the 500–700 nm range, whereas this drop in response is absent in the solar cells incorporating V-series HTMs. Significant EQE response drop in the long wavelength range of P3HT device was observed in previous studies [20,21] and ascribed to

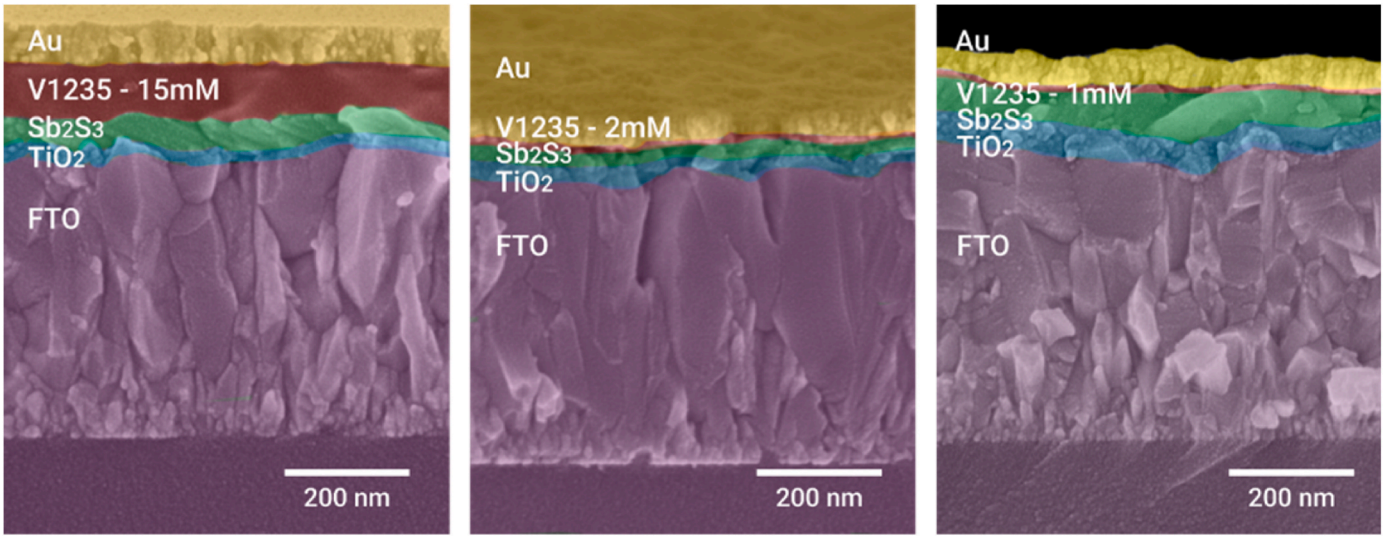

Fig. 4. SEM cross-sectional images of solar cells with HTM V1235 concentrations of 15 mM, 2 mM and 1 mM.

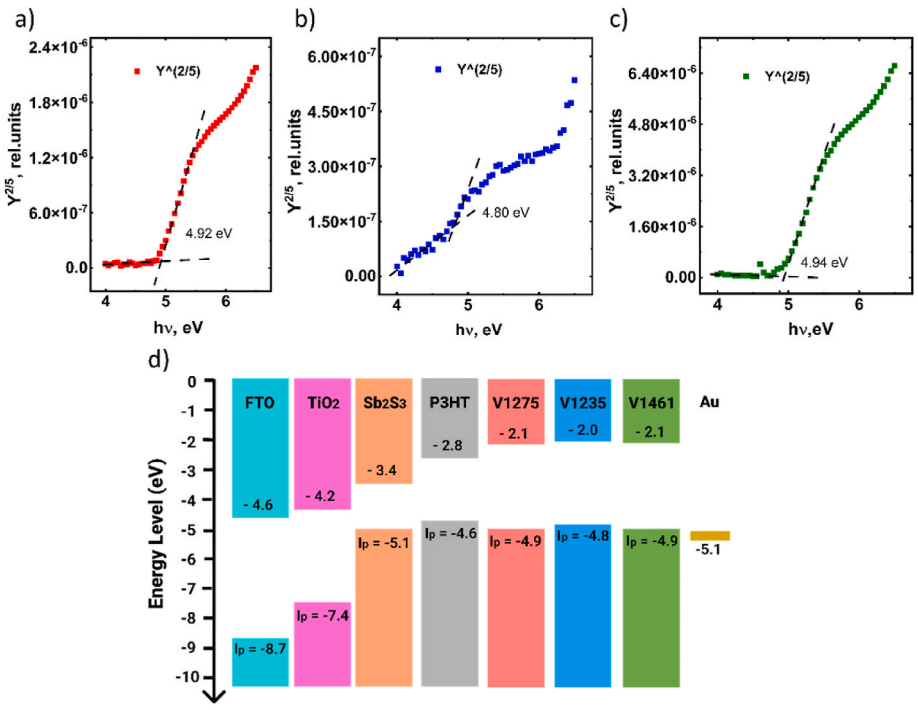

Fig. 5. Ionization potential of HTMs – a) V1275, b) V1235, c) V1461 as measured by the photoelectron yield spectroscopy method. d) Energy band diagram of Sb_2S_3 solar cells with all the constituent layers.

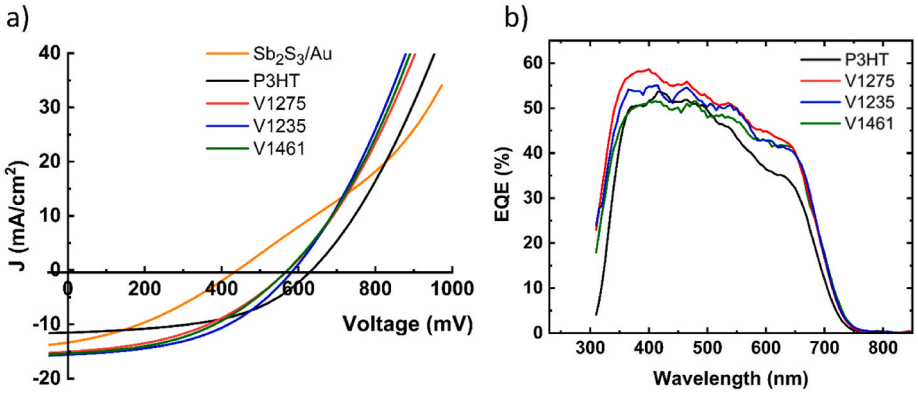

Fig. 6. a) J-V characteristics of champion Sb_2S_3 solar cells without an HTM and with optimized HTMs thicknesses for cells with P3HT, V1275, V1235, and V1461. b) EQE curves of Sb_2S_3 solar cells with different HTMs.

Table 3
Solar cell performance parameters of champion Sb_2S_3 solar cells fabricated without an HTM and with HTMs - P3HT, V1275, V1235 and V1461.

HTM	HTM conc. [mM]	V_{OC} [mV]	J_{SC} [mA/cm^2]	FF [%]	PCE [%]	R_S [Ω. cm^2]	R_{SH} [Ω. cm^2]
No HTM	-	450	12.8	40	2.1	3.2	210
P3HT	1 wt%	650	11.2	50	3.8	3.5	650
V1275	2	572	15.3	44	3.9	1.2	390
V1235	2	587	15.5	47	4.3	1.3	444
V1461	2	573	15.0	43	3.7	1.8	373

the parasitic absorption of ca. 100 nm thick P3HT layer (E_g of P3HT is ca. 1.8 eV). Also, a thicker P3HT layer prevents the reflection of incident light from the Au back contact which would otherwise double the optical path and increase its chance of absorption in the Sb_2S_3 layer [20, 21]. Such a concavity is missing in EQE spectra of solar cells using thinner layers of V-series HTMs. The absorption edge can be detected at around 700 nm, that is in line with the calculated bandgap value of Sb_2S_3 absorber ($E_g = 1.75$ eV). The calculated bandgap of Sb_2S_3 from the EQE curve with HTM V1235 is presented in SI, in Fig. S6.

Solar cells with no HTM, and with HTMs – P3HT, V1275, V1235, V1461, are fabricated to check for the reproducibility. The resulting box plots of solar cell performance parameters (V_{OC}, J_{SC}, FF and PCE) are presented in Fig. 7. It can be seen that the J_{SC} values of the cells with new HTMs - V1275, V1235 and V1461 are higher, at around 15 mA/cm^2, compared to the cells with P3HT showing J_{SC} values of around 11–12 mA/cm^2. Higher current densities of solar cells with V-series HTMs are probably due to lower layer thicknesses and absence of parasitic absorption characteristic of P3HT. Nevertheless, the V_{OC} values of cells with new HTMs are lower (at around 570–580 mV) compared to the cells with P3HT presenting Voc at around 620–630 mV. Higher V_{OC} values in P3HT-based devices may result from favorable chemical interactions between thiophene and Sb atoms at the Sb_2S_3/P3HT interface, enhancing carrier collection and suppressing charge recombination.

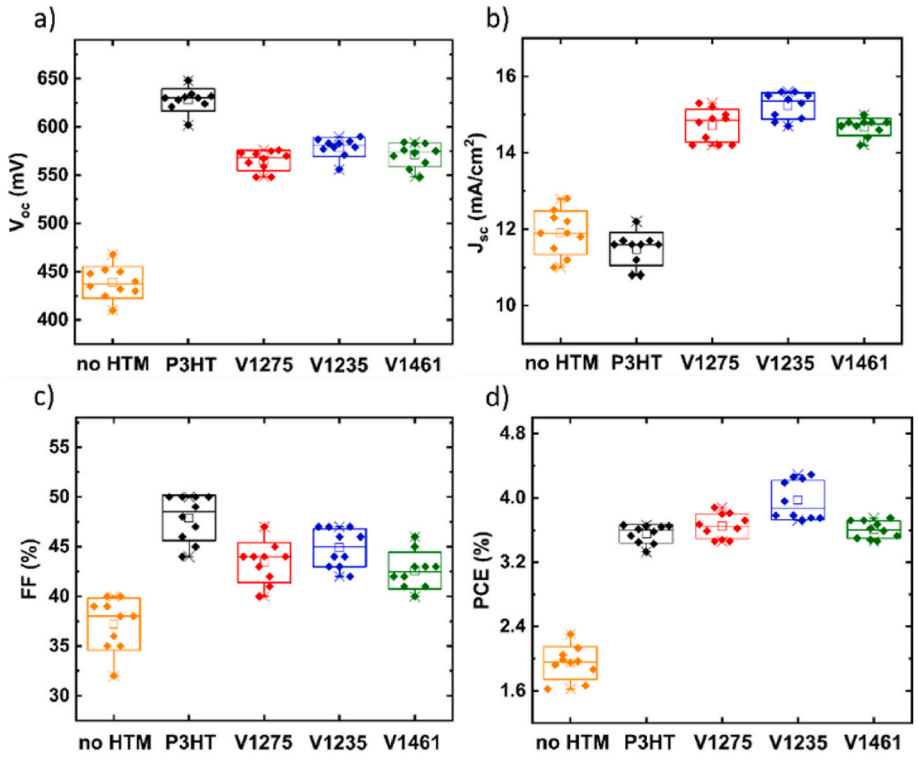

Fig. 7. Box-plot diagrams of performance parameters of the fabricated solar cell devices without any HTM and incorporating various HTMs (P3HT, V1275, V1235, and V1461).

Additionally, V-series HTMs with a 15–20 nm thickness may enable direct Au contact with the absorber at some points, unlike P3HT (ca. 100 nm). Intriguingly, lower V_{OC} values were observed in perovskite cells using V-series HTMs with larger layer thickness (120–150 nm) compared to Spiro-OMeTAD [49]. Thus, substituting traditional HTMs with V-series HTMs yields lower V_{OC} values in both perovskite and Sb_2S_3 solar cells. The PCEs of solar cells using V1275 and V1235 as HTMs outperform the PCEs of P3HT based cells. It should be noted that the spread of all the device parameters (V_{OC}, J_{SC}, FF and PCE) is reasonably small, demonstrating a good reproducibility of the fabricated solar cells. The long-term stability of unencapsulated solar cell devices with various HTMs was assessed, the aged solar cell efficiencies are compared to that of as-prepared devices (Table S2, in SI). It appears that devices with V1275 and V1235 show better stability compared to that with P3HT, but the device with V1461, which has the longest aliphatic chain in its structure, is the most unstable.

The measured transmittance spectra of the HTM layers (P3HT, V1275, V1235, and V1461) deposited on a glass/FTO substrate are shown in Fig. 8a. Parasitic absorption can be seen in case of P3HT in range of 400–650 nm which is missing from the V-series HTMs. In order to gain a better understanding of the impact of investigated HTMs on the spectral response, the total transmission spectra measurements of the fabricated solar cell devices were performed as well and are provided in SI in Fig. S7. Values of average visible transmittance (AVT), are calculated in the 400–800 nm region, for all the fabricated solar cell devices (glass/FTO/Sb_2S_3/HTM/Au) and is presented in Fig. 8b.

While the devices with P3HT and the investigated HTMs, exhibit AVT values exceeding 20%, it is observed that devices with V-series HTMs have shown enhanced transparency, with approximately 20% higher AVT compared to devices with P3HT. Here, it is important to highlight that the thickness values of the HTM films compared herein for P3HT and V1275, V1235 and V1461 are ca. 100 and 25 nm, respectively. These thicknesses have been optimized for achieving the highest efficiency in Sb_2S_3 based solar cells in each respective case. The

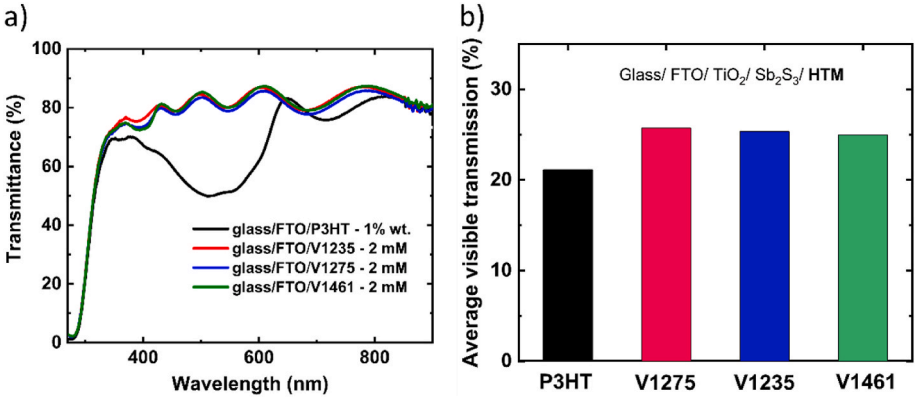

Fig. 8. a) Transmittance spectra of HTM layers (P3HT, V1275, V1235, and V1461) deposited on glass/FTO substrate, and b) calculated average visible transmittance values of solar cell devices in the range 400–800 nm incorporating different HTM layers (P3HT, V1275, V1235, and V1461).

observed improvement in transparency at the device level further validates the use of V - series HTMs in Sb_2S_3 solar cells for semi-transparent applications.

4. Conclusions

In our study, we have successfully demonstrated, for the first time, the utilization of cost-effective and transparent fluorene-based enamines - V1275, V1235 and V1461, as efficient hole transport layers in semi-transparent Sb_2S_3 based solar cells. It was demonstrated that the new V-series HTMs can boost both, the PCE as well as the average visible transmittance of USP Sb_2S_3 based devices, compared to traditional P3HT-based solar cells. While the solar cells with the conventional P3HT as HTM have yielded 3.8% efficiency and an AVT of 21%, the devices with optimized V1275, V1235, and V1461 HTM thicknesses yielded efficiencies of 3.9%, 4.3%, and 3.7%, respectively and an AVT of 25% in the spectral region 400–800 nm. The increase in the solar cell performance with new HTMs was mainly determined by substantial enhancement in the current densities of the cells. Energy level diagrams compiled using the ionization potential values measured for the cell component layers in the structure FTO/TiO_2/Sb_2S_3/HTM/Au, reveal that the new HTMs show agreeable band offsets, validating them as efficient HTMs for Sb_2S_3 solar cells. The improvement in the PCE of the cells was explained in correlation with the band alignment between HTM layer and Sb_2S_3 absorber, the length of the HTM aliphatic chain and its resulting carrier mobility in HTM and the passivation effect at the HTM - absorber back interface. These results provide new knowledge on the development of semi-transparent Sb_2S_3 based solar cells incorporating alternative HTMs, opening new opportunities to expand the application range of semi-transparent devices (such as solar windows) as well as offering broader possibilities to implement the developed processes in other emerging inorganic PV materials and device concepts.

CRediT authorship contribution statement

Nimish Juneja: Writing – original draft, Visualization, Validation, Methodology, Data curation, Conceptualization. **Sarune Daskeviciute-Geguziene:** Writing – review & editing, Validation, Methodology. **Nicolae Spalatu:** Writing – review & editing, Visualization, Supervision, Methodology, Formal analysis. **Sreekanth Mandati:** Writing – review & editing, Conceptualization. **Atanas Katerski:** Validation, Methodology. **Raitis Grzibovskis:** Writing – review & editing, Validation, Methodology. **Aivars Vembris:** Writing – review & editing, Methodology. **Smagul Karazhanov:** Writing – review & editing. **Vytautas Getautis:** Writing – review & editing, Validation, Methodology, Conceptualization. **Malle Krunks:** Writing – review & editing, Supervision, Methodology, Conceptualization. **Ilona Oja Acik:** Writing – review & editing, Project administration, Funding acquisition, Conceptualization.

Declaration of competing interest

The authors declare that they have no known competing financial interests or personal relationships that could have appeared to influence the work reported in this paper.

Data availability

Data will be made available on request.

Acknowledgments

The “Development of Semi-Transparent Bifacial Thin Film Solar Cells for Innovative Applications” benefits from a 999372 € grant from Iceland, Liechtenstein and Norway through the EEA Grants. The aim of the project is to develop new approach based on novel materials and structures and production technologies, which are the key to further increase the share, and range of application of PV in areas with sub-average sunlight, including Baltic and Nordic countries. Therefore, development of resource saving, cost-effective and efficient PV devices is a primary challenge of this project. Project contract with the Research Council of Lithuania (LMTLT) No is S-BMT-21-1(LT08-2-LMT-K-01-003). Department of Materials and Environmental Technology, Tallinn University of Technology has received funding from the Estonian Research Council, projects PRG627 “Antimony chalcogenide thin films for next-generation semi-transparent solar cells applicable in electricity producing windows” and PSG689 “Bismuth Chalcogenide Thin-Film Disruptive Green Solar Technology for Next Generation Photovoltaics”. The research was partially funded by the Estonian Centre of Excellence project TK141 (TAR16016EK) “Advanced materials and high-technology devices for energy recuperation systems”, the European Union’s Horizon 2020 ERA Chair project 5GSOLAR (grant agreement No. 952509). Institute of Solid-State Physics, University of Latvia has received funding from the European Union’s Horizon 2020 Framework Programme H2020-WIDESPREAD-01-2016-2017-TeamingPhase2 under grant agreement No. 739508, project CAMART^2. The article is also based upon work from COST Action ’’Research and International Networking on Emerging Inorganic Chalcogenides for Photovoltaics (RENEW-PV)’’, CA21148, supported by COST (European Cooperation in Science and Technology). The authors thank Dr. Tadas Malinauskas and Dr. Valdek Mikli for their support in preparation and characterization of the samples.

Appendix A. Supplementary data

Supplementary data to this article can be found online at https://doi.org/10.1016/j.mssp.2023.107934.

References

[1] T.D. Lee, A.U. Ebong, A review of thin film solar cell technologies and challenges, Renew. Sustain. Energy Rev. 70 (2017) 1286–1297, https://doi.org/10.1016/j.rser.2016.12.028.
[2] J. Ramanujam, D.M. Bishop, T.K. Todorov, O. Gunawan, J. Rath, R. Nekovei, E. Artegiani, A. Romeo, Flexible CIGS, CdTe and a-Si:H based thin film solar cells: a review, Prog. Mater. Sci. 110 (2020), 100619, https://doi.org/10.1016/j.pmatsci.2019.100619.
[3] N. Mufti, T. Amrillah, A. Taufiq, Aripriharta Sunaryono, M. Diantoro, Zulhadjri, H. Nur, Review of CIGS-based solar cells manufacturing by structural engineering, Sol. Energy 207 (2020) 1146–1157, https://doi.org/10.1016/j.solener.2020.07.065.
[4] J. Ramanujam, U.P. Singh, Copper indium gallium selenide based solar cells – a review, Energy Environ. Sci. 10 (2017) 1306–1319, https://doi.org/10.1039/C7EE00826K.
[5] L. El Chaar, L.A. lamont, N. El Zein, Review of photovoltaic technologies, Renew. Sustain. Energy Rev. 15 (2011) 2165–2175, https://doi.org/10.1016/j.rser.2011.01.004.
[6] S. Philipps, F. Ise, W. Warmuth, P. Projects GmbH, Photovoltaics report, n.d, www.ise.fraunhofer.de.
[7] T.D.C. Hobson, H. Shiel, C.N. Savory, J.E.N. Swallow, L.A.H. Jones, T. J. Featherstone, M.J. Smiles, P.K. Thakur, T.-L. Lee, B. Das, C. Leighton, G. Zoppi, V.R. Dhanak, D.O. Scanlon, T.D. Veal, K. Durose, J.D. Major, P-type conductivity in Sn-doped Sb $_2$ Se $_3$, J. Phys.: Energy 4 (2022), 045006, https://doi.org/10.1088/2515-7655/ac91a6.
[8] R. Krautmann, N. Spalatu, R. Josepson, R. Nedzinskas, R. Kondrotas, R. Gržibovskis, A. Vembris, M. Krunks, I. Oja Acik, Low processing temperatures explored in Sb2S3 solar cells by close-spaced sublimation and analysis of bulk and interface related defects, Sol. Energy Mater. Sol. Cell. 251 (2023), 112139, https://doi.org/10.1016/j.solmat.2022.112139.
[9] M. Koltsov, R. Krautmann, A. Katerski, N. Maticiuc, M. Krunks, I. Oja Acik, N. Spalatu, A post-deposition annealing approach for organic residue control in TiO $_2$ and its impact on Sb $_2$ Se $_3$/TiO $_2$ device performance, Faraday Discuss 239 (2022) 273–286, https://doi.org/10.1039/D2FD00064D.
[10] S. Barthwal, R. Kumar, S. Pathak, Present status and future perspective of antimony chalcogenide (Sb2X3) photovoltaics, ACS Appl. Energy Mater. 5 (2022) 6545–6585, https://doi.org/10.1021/acsaem.2c00420.
[11] J.S. Eensalu, A. Katerski, E. Kärber, I. Oja Acik, A. Mere, M. Krunks, Uniform Sb $_2$ S $_3$ optical coatings by chemical spray method, Beilstein J. Nanotechnol. 10 (2019) 198–210, https://doi.org/10.3762/bjnano.10.18.
[12] S. Wang, Y. Zhao, B. Che, C. Li, X. Chen, R. Tang, J. Gong, X. Wang, G. Chen, T. Chen, J. Li, X. Xiao, A novel multi-sulfur source collaborative chemical bath

deposition technology enables 8%-efficiency Sb_2S_3 planar solar cells, Adv. Mater. 34 (2022), 2206242, https://doi.org/10.1002/adma.202206242.
[13] Y. Zhao, S. Wang, C. Jiang, C. Li, P. Xiao, R. Tang, J. Gong, G. Chen, T. Chen, J. Li, X. Xiao, Regulating energy band alignment via alkaline metal fluoride assisted solution post-treatment enabling $Sb_2(S,Se)_3$ solar cells with 10.7% efficiency, Adv. Energy Mater. 12 (2022), https://doi.org/10.1002/aenm.202103015.
[14] Y. Zhao, S. Wang, C. Li, B. Che, X. Chen, H. Chen, R. Tang, X. Wang, G. Chen, T. Wang, J. Gong, T. Chen, X. Xiao, J. Li, Regulating deposition kinetics *via* a novel additive-assisted chemical bath deposition technology enables fabrication of 10.57%-efficiency Sb_2Se_3 solar cells, Energy Environ. Sci. 15 (2022) 5118–5128, https://doi.org/10.1039/D2EE02261C.
[15] C. Lan, J. Luo, H. Lan, B. Fan, H. Peng, J. Zhao, H. Sun, Z. Zheng, G. Liang, P. Fan, Enhanced charge extraction of Li-doped TiO2 for efficient thermal-evaporated Sb2S3 thin film solar cells, Materials 11 (2018) 355, https://doi.org/10.3390/ma11030355.
[16] P. Büttner, F. Scheler, C. Pointer, D. Döhler, M.K.S. Barr, A. Koroleva, D. Pankin, R. Hatada, S. Flege, A. Manshina, E.R. Young, I. Mínguez-Bacho, J. Bachmann, Adjusting interfacial chemistry and electronic properties of photovoltaics based on a highly pure Sb_2S_3 absorber by atomic layer deposition, ACS Appl. Energy Mater. 2 (2019) 8747–8756, https://doi.org/10.1021/acsaem.9b01721.
[17] J.S. Eensalu, A. Katerski, E. Kärber, L. Weinhardt, M. Blum, C. Heske, W. Yang, I. Oja Acik, M. Krunks, Semitransparent Sb_2S_3 thin film solar cells by ultrasonic spray pyrolysis for use in solar windows, Beilstein J. Nanotechnol. 10 (2019) 2396–2409, https://doi.org/10.3762/bjnano.10.230.
[18] S. Wang, Y. Zhao, B. Che, C. Li, X. Chen, R. Tang, J. Gong, X. Wang, G. Chen, T. Chen, J. Li, X. Xiao, A novel multi-sulfur source collaborative chemical bath deposition technology enables 8%-efficiency Sb_2S_3 planar solar cells, Adv. Mater. 34 (2022), 2206242, https://doi.org/10.1002/adma.202206242.
[19] Y.C. Choi, D.U. Lee, J.H. Noh, E.K. Kim, S. Il Seok, Highly improved Sb_2S_3 sensitized-inorganic-organic heterojunction solar cells and quantification of traps by deep-level transient spectroscopy, Adv. Funct. Mater. 24 (2014) 3587–3592, https://doi.org/10.1002/adfm.201304238.
[20] N. Juneja, S. Mandati, A. Katerski, N. Spalatu, S. Daskeviciute-Geguziene, A. Vembris, S. Karazhanov, V. Getautis, M. Krunks, I. Oja Acik, Sb_2S_3 solar cells with a cost-effective and dopant-free fluorene-based enamine as a hole transport material, Sustain. Energy Fuels 6 (2022) 3220–3229, https://doi.org/10.1039/D2SE00356B.
[21] S. Mandati, N. Juneja, A. Katerski, A. Jegorovė, R. Grzibovskis, A. Vembris, T. Dedova, N. Spalatu, A. Magomedov, S. Karazhanov, V. Getautis, M. Krunks, I. Oja Acik, 4.9% efficient Sb_2S_3 solar cells from semitransparent absorbers with fluorene-based thiophene-terminated hole conductors, ACS Appl. Energy Mater. (2023), https://doi.org/10.1021/acsaem.2c04097.
[22] E. Moustafa, J.G. Sánchez, L.F. Marsal, J. Pallarès, Stability enhancement of high-performance inverted polymer solar cells using ZnO electron interfacial layer deposited by intermittent spray pyrolysis approach, ACS Appl. Energy Mater. 4 (2021) 4099–4111, https://doi.org/10.1021/acsaem.1c00455.
[23] J. Han, X. Pu, H. Zhou, Q. Cao, S. Wang, Z. He, B. Gao, T. Li, J. Zhao, X. Li, Synergistic effect through the introduction of inorganic zinc halides at the interface of TiO_2 and Sb_2S_3 for high-performance Sb_2S_3 planar thin-film solar cells, ACS Appl. Mater. Interfaces 12 (2020) 44297–44306, https://doi.org/10.1021/acsami.0c11550.
[24] H.-J. Jo, S.H. Kim, J.S. Kim, S.-J. Lee, D.-H. Kim, Time-resolved photocurrent of an organic-inorganic hybrid solar cell based on Sb2S3, J. Kor. Phys. Soc. 69 (2016) 541–546, https://doi.org/10.3938/jkps.69.541.
[25] J. Luo, W. Xiong, G. Liang, Y. Liu, H. Yang, Z. Zheng, X. Zhang, P. Fan, S. Chen, Fabrication of Sb2S3 thin films by magnetron sputtering and post-sulfurization/selenization for substrate structured solar cells, J. Alloys Compd. 826 (2020), 154235, https://doi.org/10.1016/j.jallcom.2020.154235.
[26] M.Y. Versavel, J.A. Haber, Structural and optical properties of amorphous and crystalline antimony sulfide thin-films, Thin Solid Films 515 (2007) 7171–7176, https://doi.org/10.1016/j.tsf.2007.03.043.
[27] E. Gnenna, N. Khemiri, M. Kong, M. Isabel Alonso, M. Kanzari, Effect of vacuum annealing on the properties of one step thermally evaporated Sb_2S_3 thin films for photovoltaic applications, Eur. Phys. J. Appl. Phys. 96 (2021), 20301, https://doi.org/10.1051/epjap/2021210101.
[28] C.P. Liu, H.E. Wang, T.W. Ng, Z.H. Chen, W.F. Zhang, C. Yan, Y.B. Tang, I. Bello, L. Martinu, W.J. Zhang, S.K. Jha, Hybrid photovoltaic cells based on ZnO/Sb2S3/P3HT heterojunctions, Phys. Status Solidi 249 (2012) 627–633, https://doi.org/10.1002/pssb.201147393.
[29] L. Guo, B. Zhang, S. Li, Q. Zhang, M. Buettner, L. Li, X. Qian, F. Yan, Scalable and efficient Sb_2S_3 thin-film solar cells fabricated by close space sublimation, Apl. Mater. 7 (2019), 041105, https://doi.org/10.1063/1.5090773.
[30] Y. Zeng, F. Liu, M. Green, X. Hao, Fabrication of Sb_2S_3 planar thin film solar cells with closed-space sublimation method, in: 2018 IEEE 7th World Conference on Photovoltaic Energy Conversion (WCPEC) (A Joint Conference of 45th IEEE PVSC, 28th PVSEC & 34th EU PVSEC), IEEE, 2018, https://doi.org/10.1109/PVSC.2018.8547305, 0870–0872.
[31] J. Han, S. Wang, J. Yang, S. Guo, Q. Cao, H. Tang, X. Pu, B. Gao, X. Li, Solution-Processed Sb_2S_3 planar thin film solar cells with a conversion efficiency of 6.9% at an open circuit voltage of 0.7 V achieved via surface passivation by a $SbCl_3$ interface layer, ACS Appl. Mater. Interfaces 12 (2020) 4970–4979, https://doi.org/10.1021/acsami.9b15148.
[32] P. Büttner, F. Scheler, C. Pointer, D. Döhler, T. Yokosawa, E. Spiecker, P.P. Boix, E. R. Young, I. Mínguez-Bacho, J. Bachmann, ZnS ultrathin interfacial layers for optimizing carrier management in Sb_2S_3 -based photovoltaics, ACS Appl. Mater. Interfaces 13 (2021) 11861–11868, https://doi.org/10.1021/acsami.0c21365.
[33] S.-J. Lee, S.-J. Sung, K.-J. Yang, J.-K. Kang, J.Y. Kim, Y.S. Do, D.-H. Kim, Approach to transparent photovoltaics based on wide band gap Sb_2S_3 absorber layers and optics-based device optimization, ACS Appl. Energy Mater. 3 (2020) 12644–12651, https://doi.org/10.1021/acsaem.0c02552.
[34] E. Zimmermann, T. Pfadler, J. Kalb, J.A. Dorman, D. Sommer, G. Hahn, J. Weickert, L. Schmidt-Mende, Toward high-efficiency solution-processed planar heterojunction Sb_2S_3 solar cells, Adv. Sci. 2 (2015), 1500059, https://doi.org/10.1002/advs.201500059.
[35] H. Ning, H. Guo, J. Zhang, X. Wang, X. Jia, J. Qiu, N. Yuan, J. Ding, Enhancing the efficiency of Sb2S3 solar cells using dual-functional potassium doping, Sol. Energy Mater. Sol. Cell. 221 (2021), 110816, https://doi.org/10.1016/j.solmat.2020.110816.
[36] D.-H. Kim, S.-J. Lee, M.S. Park, J.-K. Kang, J.H. Heo, S.H. Im, S.-J. Sung, Highly reproducible planar Sb_2S_3 -sensitized solar cells based on atomic layer deposition, Nanoscale 6 (2014) 14549–14554, https://doi.org/10.1039/C4NR04148H.
[37] J. Zhong, X. Zhang, Y. Zheng, M. Zheng, M. Wen, S. Wu, J. Gao, X. Gao, J.-M. Liu, H. Zhao, High efficiency solar cells as fabricated by Sb_2S_3 -modified TiO_2 nanofibrous networks, ACS Appl. Mater. Interfaces 5 (2013) 8345–8350, https://doi.org/10.1021/am401273r.
[38] R. Nie, S. Il Seok, Efficient antimony-based solar cells by enhanced charge transfer, Small Methods 4 (2020), 1900698, https://doi.org/10.1002/smtd.201900698.
[39] J.A. Chang, S.H. Im, Y.H. Lee, H. Kim, C.-S. Lim, J.H. Heo, S. Il Seok, Panchromatic photon-harvesting by hole-conducting materials in inorganic–organic heterojunction sensitized-solar cell through the formation of nanostructured electron channels, Nano Lett. 12 (2012) 1863–1867, https://doi.org/10.1021/nl204224v.
[40] X. Jin, Y. Yuan, C. Jiang, H. Ju, G. Jiang, W. Liu, C. Zhu, T. Chen, Solution processed NiOx hole-transporting material for all-inorganic planar heterojunction Sb2S3 solar cells, Sol. Energy Mater. Sol. Cell. 185 (2018) 542–548, https://doi.org/10.1016/j.solmat.2018.06.017.
[41] Y. Itzhaik, O. Niitsoo, M. Page, G. Hodes, Sb_2S_3 -sensitized nanoporous TiO_2 solar cells, J. Phys. Chem. C 113 (2009) 4254–4256, https://doi.org/10.1021/jp900302b.
[42] J.A. Christians, P.V. Kamat, Trap and transfer. Two-step hole injection across the Sb_2S_3/CuSCN interface in solid-state solar cells, ACS Nano 7 (2013) 7967–7974, https://doi.org/10.1021/nn403058f.
[43] L. Zhang, C. Jiang, C. Wu, H. Ju, G. Jiang, W. Liu, C. Zhu, T. Chen, V_2O_5 as hole transporting material for efficient all inorganic Sb_2S_3 solar cells, ACS Appl. Mater. Interfaces 10 (2018) 27098–27105, https://doi.org/10.1021/acsami.8b09843.
[44] T.P.I. Saragi, T. Spehr, A. Siebert, T. Fuhrmann-Lieker, J. Salbeck, Spiro compounds for organic optoelectronics, Chem. Rev. 107 (2007) 1011–1065, https://doi.org/10.1021/cr0501341.
[45] J.P. Chen, H. Tanabe, X.-C. Li, T. Thoms, Y. Okamura, K. Ueno, Novel organic hole transport material with very high Tg for light-emitting diodes, Synth. Met. 132 (2003) 173–176, https://doi.org/10.1016/S0379-6779(02)00203-5.
[46] Y. Xiang, H. Guo, Z. Cai, C. Jiang, C. Zhu, Y. Wu, W.-H. Zhu, T. Chen, Dopant-free hole-transporting materials for stable $Sb_2(S,Se)_3$ solar cells, Chem. Commun. 58 (2022) 4787–4790, https://doi.org/10.1039/D1CC07041J.
[47] M.L. Petrus, T. Bein, T.J. Dingemans, P. Docampo, A low cost azomethine-based hole transporting material for perovskite photovoltaics, J. Mater. Chem. A Mater. 3 (2015) 12159–12162, https://doi.org/10.1039/C5TA03046C.
[48] F. Machui, M. Hösel, N. Li, G.D. Spyropoulos, T. Ameri, R.R. Søndergaard, M. Jørgensen, A. Scheel, D. Gaiser, K. Kreul, D. Lenssen, M. Legros, N. Lemaitre, M. Vilkman, M. Välimäki, S. Nordman, C.J. Brabec, F.C. Krebs, Cost analysis of roll-to-roll fabricated ITO free single and tandem organic solar modules based on data from manufacture, Energy Environ. Sci. 7 (2014) 2792, https://doi.org/10.1039/C4EE01222D.
[49] S. Daskeviciute, C. Momblona, K. Rakstys, A.A. Sutanto, M. Daskeviciene, V. Jankauskas, A. Gruodis, G. Bubniene, V. Getautis, M.K. Nazeeruddin, Fluorene-based enamines as low-cost and dopant-free hole transporting materials for high performance and stable perovskite solar cells, J. Mater. Chem. A Mater. 9 (2021) 301–309, https://doi.org/10.1039/D0TA08452B.
[50] F. Laquai, D. Andrienko, R. Mauer, P.W.M. Blom, Charge carrier transport and photogeneration in P3HT:PCBM photovoltaic blends, Macromol. Rapid Commun. 36 (2015) 1001–1025, https://doi.org/10.1002/marc.201500047.
[51] J. Santos, J. Calbo, R. Sandoval-Torrientes, I. García-Benito, H. Kanda, I. Zimmermann, J. Aragó, M.K. Nazeeruddin, E. Ortí, N. Martín, Hole-transporting materials for perovskite solar cells employing an anthradithiophene core, ACS Appl. Mater. Interfaces 13 (2021) 28214–28221, https://doi.org/10.1021/acsami.1c05890.